Functionalized High-Speed Magnon Polaritons Resulting from Magnonic Antenna Effect

Kenta Kato,[1] Tomohiro Yokoyama,[1,*] and Hajime Ishihara[1,2,3,†]

[1] *Department of Material Engineering Science, Graduate School of Engineering Science, Osaka University, 1-3 Machikaneyama, Toyonaka, Osaka 560-8531, Japan*

[2] *Department of Physics and Electronics, Graduate School of Engineering, Osaka Prefecture University, 1-1 Gakuen-cho, Naka-ku, Sakai, Osaka 599-8531, Japan*

[3] *Center for Quantum Information and Quantum Biology, Osaka University, 1-3 Machikaneyama, Toyonaka, Osaka 560-8531, Japan*

(Received 12 October 2021; revised 5 December 2022; accepted 3 February 2023; published 10 March 2023)

Magnon polaritons (MPs) refer to a light-magnon coupled state, which have the potential to act as information carriers, possibly enabling charge-free computation. However, light-magnon coupling is inherently weak. To achieve sufficiently strong coupling, a large ferromagnet or coupling with a microwave cavity is necessary. Thus, we theoretically propose a 100 nm YIG/1 μm GGG/500 μm YIG structure as a fundamental platform for magnonic and magnon-optical information storage devices to address the aforementioned issues. Furthermore, we discuss the transport properties of the MPs. Owing to the waveguide modes formed by the dielectric constant of the structure, the magnons placed in a nanometer-thin layer are strongly coupled with light. In addition, a longitudinal magnon-magnon coupling between thin and thick magnetic layers yields rich functionalities and a large magnon density to the thick-layer MPs due to the "magnonic antenna effect." Hence, a large, direction-switchable magnon current in the thin layer is observed. The proposed structure indicates a longer coherence length and suitable figure of merit for the magnonic antenna effect. Therefore, the findings of this study would enable the integration of ferromagnetic micro- and nanostructures for MP-based information devices without any restrictions due to cavities.

DOI: 10.1103/PhysRevApplied.19.034035

I. INTRODUCTION

In magnetic materials, elementary excitation arises from the collective motion of spin precession; this phenomenon, which is equivalent to a quasiparticle, is called a spin wave or magnon. A magnon is a potentially viable candidate for low-energy-consumption devices because it can carry [1–4], process [2,5,6], and store [7] spin information without charge carrier transport. The spin current of magnons is proportional to the density of excited magnons ρ_m and their group velocity v_g. However, there exist two significant issues that affect the efficiency of magnonic devices: (i) the increase in magnon current with increasing density and velocity, and (ii) switchable control over current direction. However, typical magnon densities are significantly lower than the typical electron density in metals, and the typical velocity of a magnon is also considerably lower than the Fermi velocity of electrons. Thus, to overcome these issues, recent studies have focused on engineering magnon velocity [8,9] and transport [10–12].

One method to increase the velocity of magnons is to form magnon polaritons (MPs) via strong coupling between magnons and microwaves [13–15]. Magnon-light coupling is significantly weaker than the coupling between an electric dipole and light. Recent studies have achieved ultra-strong coupling for MPs using optical cavities, and the significant splitting of the dispersion relation of magnetic microspheres has been reported [14,15]. Such cavity-based MPs in magnetic microspheres exhibit rich properties, such as bistability [16,17], coherent perfect absorption [18,19], level attraction [20–23], microwave Hall effect [24], and information communication between magnetic segments in cavities [25–29]. However, to ensure information transport via magnons, it is necessary to achieve strongly coupled MPs, further referred to as strong MPs, in one- or two-dimensional integrable magnetic materials.

Several systems have been studied with the aim of discovering applications of devices with strong MPs using cavities. However, contemporary studies have not exploited the potential of the interplay between the spatial

*E-mail me at: yokoyama.t.es@osaka-u.ac.jp
†E-mail me at: ishihara.h.es@osaka-u.ac.jp

degrees of freedom of the magnons and the radiation field. For its incorporation, a multilayered two-dimensional magnetic film has an attractive potential, where the spatial profiles of the magnon wave and radiation field and their interplay are considered key components. Subsequently, a nonlocal treatment for the microwave response from magnons can be formulated. This approach, which considers the nonlocal response of magnons to the radiation field, provides an application prospect for strong MPs and is expected to offer several degrees of freedom in the spatial design of sample structures.

In this study we propose a multilayered structure of magnetic and dielectric materials, formulate a nonlocal response theory for magnons, and discuss the dispersion relation of MPs. Our formulation of the nonlocal theory is based on the quantum microscopic perspective of magnons. Magnon excitations are coupled with electromagnetic fields by following the constitutive and Maxwell's equations. (This scheme can be extended to a nonlinear magnon response in a straightforward manner.) The spatial interplay between magnons and the field is designed under both dielectric and magnetic environments. The proposed multilayered structure is shown in Fig. 1. The structure comprises of thin (approximately 100 nm) and thick (approximately 500 μm) magnetic layers. The thin layer can be processed to fabricate integrable magnonic circuits. The two magnetic layers are separated by a thin dielectric layer of an appropriate thickness (approximately 1 μm), which should be much greater than the penetration length of the magnon wave functions. In this structure, we reveal that the MPs even in a circuit-fabricated thin layer can have rich transport properties due to a transcription of the thick-layer MP properties. This transcription can be termed as the "magnonic antenna effect." Figure 1(a) shows the model considered in the present study, while Fig. 1(b) shows an imaginary processed structure.

The proposed structure is based on three important concepts. First, the "waveguide modes" formed by the multilayer interfaces enhance the strength of the MPs in the thin magnetic layer. Second, the thick layers hold the high density of excited magnons and rich functionalities for the magnon transport, such as the switching function of transport direction. Third, an interlayer (longitudinal) magnon-magnon interaction transfers the magnon excitations from the thick layer to the thin layer and transcribes the properties of the thick-layer MPs to the thin-layer MPs. In this paper we discuss these three concepts by considering several structures. For the second and third concepts, we introduce the magnonic antenna effect. The waveguide modes play the role of cavities and enhance the light-magnon couplings in both magnetic layers. Furthermore, the waveguide modes can be utilized for a conversion between the microwave and optical photons [30,31] and communication between the magnonic materials [32]. In this study we utilize the waveguide modes and magnonic antenna effect to obtain a large density and rich properties of MPs even in circuits fabricated of thin layers. Thus, to utilize the dispersion of the MPs at a large in-plane wave number $k_{\parallel}$ in the waveguide modes, the total thickness of the structure should be less than several hundreds of micrometers.

The separation of magnetic layers by the dielectric layer is essential for our proposal to achieve circuit-integrable MPs having rich functionalities. Since typical magnons have wavelengths in the millimeter scale, surface etching

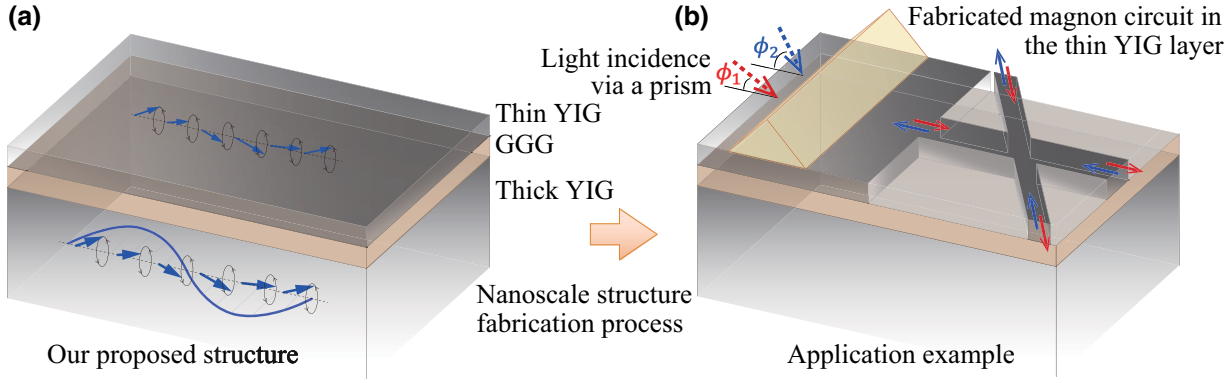

FIG. 1. Schematic of the proposed multilayer structure for magnonic devices. (a) Proposed structure comprising thin yttrium iron garnet (YIG), thin gadolinium gallium garnet (GGG), and thick YIG layers. The thick YIG layer acts as an antenna to capture photons via the formed waveguide modes. The photons are coupled with the magnons in the thin YIG layer via the magnon-magnon interaction. Thus, the thin-layer magnons can form polaritons. (b) Imaginary processed structure. Even when a thin YIG layer is used to the fabricate circuit, the MPs in the thin YIG layer are expected to demonstrate high-speed controllable magnon transport in the circuits without any magnon current leakage owing to the functionality of the MPs. To form the polaritons using the waveguide modes, a microwave with a prism or fiber coupling is used. An X-shaped junction is presented as an example of circuit fabrication.

of a thick magnet is ineffective to control the MPs. Hence, the magnonic antenna effect is prevalent owing to the separation of the magnetic layers. A cavityless structure offers significant advantages for further development, such as MP network fabrication on a substrate and MP control using a small magnetic tip. The formulated nonlocal theory for magnons indicates that a spatial correlation between the magnons and waveguide modes results in strong MPs. Hence, a combination of the aforementioned aspects enables the realization of highly efficient and switchable solid-state devices, without the requirement of charge carrier transport.

This paper is organized as follows. In Sec. II we formulate the nonlocal response and self-consistent theory for MPs and describe a model with several magnetic and dielectric layers. In Sec. III we discuss the results of magnetic response and the dispersion relation of MPs in the multilayered structure. Furthermore, the magnon current is investigated from the dispersion relations. Finally, Sec. IV concludes the study.

II. FORMULATION AND MODEL

This section provides the formulation of a nonlocal magnetic response by magnons. The quantum description of magnons with the Holstein-Primakoff transformation [33] provides the nonperturbative and perturbative Hamiltonians. A basic linear response theory [34] is used to deduce a nonlocal susceptibility of magnons for the constitutive equation. In addition, the magnon excitation causes fluctuations in magnetizations. Hence, the magnons are coupled with the electromagnetic fields (photons) spontaneously in Maxwell's equations. By a self-consistent treatment of the constitutive and Maxwell's equations, we formulate the nonlocal response theory for a magnon. Subsequently, we apply the nonlocal theory to multilayered structures of magnetic and dielectric materials. In this study, we propose a YIG/GGG/YIG structure to investigate the magnonic antenna effect and the interlayer magnon-magnon interaction.

A. Nonlocal magnetic response

The spin wave in magnetic materials can be described by an exchange interaction. For localized electron spins $\hat{\mathbf{S}}_j$ at lattice site j of magnets, the exchange Hamiltonian can be expressed as

$$\hat{\mathcal{H}}_{\rm ex} = -\sum_{\langle i,j\rangle} J_{ij}\hat{\mathbf{S}}_i\cdot\hat{\mathbf{S}}_j, \tag{1}$$

where the exchange constant J_{ij} is finite only for the neighboring sites. In this study we consider a uniform strong magnet with $J_{ij} = J_0 > 0$ and apply the Holstein-Primakoff transformation as [33]

$$\hat{S}_j^z = S - \hat{b}_j^\dagger\hat{b}_j, \tag{2}$$

$$\hat{S}_j^- = \sqrt{2S}\hat{b}_j^\dagger\left(1-\frac{\hat{b}_j^\dagger\hat{b}_j}{2S}\right), \tag{3}$$

$$\hat{S}_j^+ = \sqrt{2S}\left(1-\frac{\hat{b}_j^\dagger\hat{b}_j}{2S}\right)\hat{b}_j, \tag{4}$$

where $\hat{S}_j^\pm = \hat{S}_j^x \pm i\hat{S}_j^y$, with bosonic creation and annihilation operators represented by $\hat{b}_j^\dagger$ and $\hat{b}_j$, respectively. On removing the ground-state energy of the ferromagnet, we obtain a transformed Hamiltonian $\hat{\mathcal{H}}_m \simeq \hat{\mathcal{H}}_{\rm ex} - (-\delta N J_0 S^2)$, where δ and N represent the number of neighboring sites and the total number of sites, respectively, and S is the size of the localized spin at each site. By taking the Fourier transform of the creation and annihilation operators, $\hat{b}_{\mathbf{k}}^\dagger = 1/\sqrt{N}\sum_j \hat{b}_j^\dagger e^{i\mathbf{k}\cdot\mathbf{R}_j}$ and $\hat{b}_{\mathbf{k}} = 1/\sqrt{N}\sum_j \hat{b}_j e^{-i\mathbf{k}\cdot\mathbf{R}_j}$, the Hamiltonian for a magnon

$$\hat{\mathcal{H}}_m = 2S\sum_{\mathbf{k}}\left[\tilde{J}(0)-\tilde{J}(\mathbf{k})\right]\hat{b}_{\mathbf{k}}^\dagger\hat{b}_{\mathbf{k}} \tag{5}$$

is obtained. The boson describes the spin wave quantum or the so-called magnon, while $\tilde{J}(\mathbf{k}) = \sum_{\langle j\rangle} J_0 e^{-i\mathbf{k}\cdot\mathbf{R}_j}$ describes the excitation energy of the magnons. The summations for $\hat{b}_{\mathbf{k}}^\dagger$ and $\hat{b}_{\mathbf{k}}$ are taken for all sites, whereas the summation for $\tilde{J}(\mathbf{k})$ is taken for all neighboring sites from $\mathbf{R}_j$. The constant term can be reduced without a loss of generality. The exchange interaction originates from the Coulomb interaction between the localized electrons that is a part of the longitudinal electric fields. The dipole-dipole interaction between the magnons is also mediated by the longitudinal field. In our formulation, the former is included in the Hamiltonian, whereas the latter is considered in the Maxwell's equations.

In a magnetic field the magnon excitation energy is modulated due to the Zeeman effect $\hat{\mathcal{H}}_Z = -g\mu_B\mu_0\sum_j \hat{\mathbf{S}}_j\cdot\mathbf{H}(\mathbf{r}_j,t)$, where μ_B is the Bohr magneton and g is the g factor. The magnetic field $\mathbf{H}(\mathbf{r},t)$ consists of an external static field $\mathbf{H}_0$, an incident microwave $\mathbf{h}_{\rm inc}(\mathbf{r},t)$, and a response field $\mathbf{h}_{\rm res}(\mathbf{r},t)$. The response field is generated by the excited magnons. The total Hamiltonian is expressed as $\hat{\mathcal{H}} = \hat{\mathcal{H}}_m + \hat{\mathcal{H}}_Z$. On introducing $\mathbf{h}(\mathbf{r},t) = \mathbf{h}_{\rm inc}(\mathbf{r},t) + \mathbf{h}_{\rm res}(\mathbf{r},t)$, we divide the total Hamiltonian into static nonperturbative and time-dependent perturbative Hamiltonians as

$$\hat{\mathcal{H}}_0 = \sum_{\mathbf{k}} E_{\mathbf{k}}\hat{b}_{\mathbf{k}}^\dagger\hat{b}_{\mathbf{k}}, \tag{6}$$

$$\hat{\mathcal{H}}'(t) = -g\mu_B\mu_0 \sum_j \hat{\mathbf{S}}_j \cdot \mathbf{h}(\mathbf{r}_j, t), \tag{7}$$

respectively, with the magnon excitation energy being

$$\begin{aligned} E_{\mathbf{k}} &= 2S[\tilde{J}(0) - \tilde{J}(\mathbf{k})] + g\mu_B\mu_0|\mathbf{H}_0| \\ &\simeq \hbar\omega_M\lambda_{\mathrm{ex}}^2 k^2 + \hbar\omega_H. \end{aligned} \tag{8}$$

The magnon energy is shifted by the external field $|\mathbf{H}_0|$. Here, $\lambda_{\mathrm{ex}} = \sqrt{2S|\nabla_k^2 J(\mathbf{k})|/(\hbar\omega_M)}$ is a length scale of the exchange interaction and $\hbar\omega_M = \hbar\gamma\mu_0|\mathbf{M}_s|$ is the magnetization energy, where $\gamma = g\mu_B/\hbar$ is the gyromagnetic ratio and $\mathbf{M}_s$ is the saturation magnetization.

Based on the quantum description of magnons by the Hamiltonian $\hat{\mathcal{H}}(t) = \hat{\mathcal{H}}_0 + \hat{\mathcal{H}}'(t)$, we formulate the microscopic theory of magnon response. We assume a monotonic field incidence $\mathbf{h}_{\mathrm{inc}}(\mathbf{r}, t) = \mathbf{h}_{\mathrm{inc}}(\mathbf{r}; \omega)e^{-i\omega t}$. The constitutive equation for the magnetic response is given by

$$\mathbf{m}(\mathbf{r}_i; \omega) = \sum_j \bar{\chi}(\mathbf{r}_i, \mathbf{r}_j; \omega)\mathbf{h}(\mathbf{r}_j; \omega) \tag{9}$$

with the nonlocal susceptibility [35]. Here, $\mathbf{m}(\mathbf{r}_i; \omega)$ denotes the deviation of the magnetization from the saturation magnetization. The susceptibility is obtained by the linear response theory [34] as

$$\begin{aligned} \bar{\chi}(\mathbf{r}_i, \mathbf{r}_j; \omega) = -\frac{\mu_0}{v} \sum_n \Bigg[&\frac{\boldsymbol{\mu}_{0n}(\mathbf{r}_i)\{\boldsymbol{\mu}_{n0}(\mathbf{r}_j)\}^t}{E_n - \hbar\omega - i\gamma_m} \\ &+ \frac{\boldsymbol{\mu}_{n0}(\mathbf{r}_i)\{\boldsymbol{\mu}_{0n}(\mathbf{r}_j)\}^t}{E_n + \hbar\omega + i\gamma_m} \Bigg], \end{aligned} \tag{10}$$

where $\boldsymbol{\mu}_{nm}(\mathbf{r}_j) = -g\mu_B\langle\mathbf{k}_n|\hat{\mathbf{S}}_j|\mathbf{k}_m\rangle$. The index n represents the eigenstate $|\mathbf{k}_n\rangle$ of $\hat{\mathcal{H}}_0$, γ_m is a nonradiative relaxation constant, and v is the volume of the unit cell for each site.

B. Layered structure

We consider the magnetic nonlocal response of magnons in a layered structure. The magnon wave functions (or spin waves) are confined owing to the pinning effect at the surfaces. The magnon states are well defined as $|n, \mathbf{k}_\parallel\rangle$ with an in-plane wave number. Then, we obtain $\sqrt{1/v}\langle 0|\hat{\mathbf{S}}_j|n, \mathbf{k}_\parallel\rangle = \sqrt{S/2}1/L\exp(i\mathbf{k}_\parallel \cdot \boldsymbol{\rho}_{j,\parallel})\phi_n(z_j)(1, -i, 0)^t$, where $\phi_n(z_j)$ is the wave function of the magnon in the z direction. For a single-layered structure, we find that $\phi_n(z_j) = \sqrt{2/d}\sin(n\pi z_j/d)$, where d and L are the thickness in the z direction and the size of the system in the x-y plane, respectively, $\boldsymbol{\rho}_{j,\parallel} = (x_j, y_j)$ is the position vectors, and S is the value of the spin. We apply the continuous approximation for the magnon wave functions. For the translational symmetry in the x-y plane, the field and magnetization are partially Fourier-transformed as $\mathbf{h}(\boldsymbol{\rho}_\parallel, z; \omega) = (1/2\pi)\int d^2\mathbf{k}_\parallel\, \tilde{\mathbf{h}}(\mathbf{k}_\parallel, z; \omega)e^{i\mathbf{k}_\parallel\cdot\boldsymbol{\rho}_\parallel}$. The constitutive equation is also rewritten as

$$\tilde{\mathbf{m}}(\mathbf{k}_\parallel, z; \omega) = \int dz'\,\bar{\chi}(\mathbf{k}_\parallel, z, z'; \omega)\tilde{\mathbf{h}}(\mathbf{k}_\parallel, z'; \omega), \tag{11}$$

where the susceptibility is represented by

$$\begin{aligned} \bar{\chi}(\mathbf{k}_\parallel, z, z'; \omega) = -\frac{\mu_0}{v} \sum_n \Bigg[&\frac{\tilde{\boldsymbol{\mu}}_n(z)\tilde{\boldsymbol{\mu}}_n^\dagger(z')}{E_{n,\mathbf{k}_\parallel} - \hbar\omega - i\gamma_m} \\ &+ \frac{\tilde{\boldsymbol{\mu}}_n^*(z)\tilde{\boldsymbol{\mu}}_n^t(z')}{E_{n,\mathbf{k}_\parallel} + \hbar\omega + i\gamma_m} \Bigg], \end{aligned} \tag{12}$$

where $\tilde{\boldsymbol{\mu}}_n(z) = g\mu_B\sqrt{S/2}\phi_n(z)(1, -i, 0)^t$. For multilayered systems, the susceptibility is expressed as a combination of Eq. (12) for the respective layers.

C. Maxwell's equations

The coupling between the magnon and electromagnetic field is described by a self-consistent relation with the nonlocal constitutive equation and the microscopic Maxwell's equations, where the spatial correlation between the magnon wave function and the electromagnetic field should be treated appropriately. The microscopic Maxwell's equations are

$$\nabla \cdot \mathbf{E} = -\frac{1}{\varepsilon_0}\nabla \cdot \mathbf{P}, \tag{13}$$

$$\nabla \times \mathbf{E} = -\frac{\partial \mathbf{B}}{\partial t}, \tag{14}$$

$$\nabla \cdot \mathbf{B} = 0, \tag{15}$$

$$\nabla \times \mathbf{B} = \varepsilon_0\mu_0\frac{\partial \mathbf{E}}{\partial t} + \mu_0\nabla \times \mathbf{M} + \mu_0\frac{\partial \mathbf{P}}{\partial t}. \tag{16}$$

Here $\mathbf{E}$, $\mathbf{B}$, $\mathbf{M}$, $\mathbf{P}$, ε_0, and μ_0 denote the total electric field, total magnetic flux density, magnetization, polarization, dielectric constant in vacuum, and permeability in vacuum, respectively. The magnons are described in terms of $\mathbf{M}(\mathbf{r})$ with the nonlocal susceptibility in Eq. (12), while the polarization is represented by the dielectric constant of each layer as $\mathbf{P}(\mathbf{r}) = \varepsilon_0\chi_E(z)\mathbf{E}(\mathbf{r})$. The dielectric constant $\varepsilon_0\chi_E(z)$ forms the TE and TM waveguide modes. We set the field propagation direction along the x-z plane $\mathbf{k} = (k_\parallel, 0, k_z)^t$. Subsequently, the y component of the magnetic (electric) field determines the reflection and transmission of the TM (TE) waveguide mode.

For the magnetic field $\mathbf{H} = \mathbf{B}/\mu_0 - \mathbf{M}$, the Maxwell's equations become

$$\nabla \times \nabla \times \mathbf{H} + \mu_0\varepsilon_0(1+\chi_E)\frac{\partial^2 \mathbf{H}}{\partial t^2} = -\mu_0\varepsilon_0(1+\chi_E)\frac{\partial^2 \mathbf{M}}{\partial t^2} + \varepsilon_0(\nabla\chi_E)\times\frac{\partial \mathbf{E}}{\partial t}. \quad (17)$$

The systems considered in this study have transverse symmetry in the x-y direction. We consider partial Fourier transformations with $\mathbf{k}_\parallel$ and ω for the magnetic fields. Here $\tilde{\mathbf{H}}(\mathbf{k}_\parallel, z; \omega) = 1/(2\pi)^{3/2}\int dxdy\int dt\mathbf{H}(\mathbf{r}, t)e^{ik_x x}e^{-i\omega t}$. The electric field is also Fourier transformed in the same manner.

We divide the field into TM and TE modes as $\tilde{\mathbf{H}} = \tilde{\mathbf{H}}^{(\mathrm{TM})} + \tilde{\mathbf{H}}^{(\mathrm{TE})}$. For the TM mode $\tilde{\mathbf{H}}^{(\mathrm{TM})} = (0, \tilde{H}_y, 0)^t$, the solution is given as

$$\tilde{\mathbf{H}}^{(\mathrm{TM})}(\mathbf{k}_\parallel, z; \omega) = \tilde{\mathbf{H}}^{(\mathrm{TM})}_{\mathrm{inc}}(\mathbf{k}_\parallel, z; \omega) + \int dz' \bar{G}^{(\mathrm{TM})}(\mathbf{k}_\parallel, z, z'; \omega)\tilde{\mathbf{M}}(\mathbf{k}_\parallel, z'; \omega) \quad (18)$$

with a dyadic Green's function

$$\bar{G}^{(\mathrm{TM})}(\mathbf{k}_\parallel, z, z'; \omega) = -\begin{pmatrix} 0 & & \\ & q(z')^2 & \\ & & 0 \end{pmatrix}\frac{ig(\mathbf{k}_\parallel, z, z'; \omega)}{2\sqrt{q(z')^2 - k_\parallel^2}}, \quad (19)$$

where $g(\mathbf{k}_\parallel, z, z'; \omega)$ is a scalar Green's function describing a scalar wave propagation from position z' in a layer to z in the same or other layers. The term $(\nabla\chi_E)\times\tilde{\mathbf{E}}$ in Eq. (17) causes a local modulation at the interfaces by a stepwise change of χ_E. However, in our formulation, the modulation is considered by the boundary conditions for $g(\mathbf{k}_\parallel, z, z'; \omega)$. In the nth layer, $z_{n-1} < z < z_n$, the wave number is $q(z) = q_n = \chi_{E,n}\omega/c$. For $z_{n-1} < z < z_n$ and $z_{m-1} < z' < z_m$, the scalar Green's function is given as

$$g(\mathbf{k}_\parallel, z, z'; \omega) = \begin{cases} \left[e^{ik_n(z-z_{n-1})} + e^{-ik_n(z-z_n)}\tilde{r}_{n+1,n}e^{ik_n d_n}\right]\tilde{t}_{n,m}A_m(z') & (n > m), \\ e^{ik_m|z-z'|} + e^{ik_m(z-z_{m-1})}B_m(z') + e^{-ik_m(z-z_m)}C_m(z') & (n = m), \\ \left[e^{-ik_n(z-z_n)} + e^{ik_n(z-z_{n-1})}\tilde{r}_{n-1,n}e^{ik_n d_n}\right]\tilde{t}_{n,m}D_m(z') & (n < m), \end{cases} \quad (20)$$

with the factors

$$A_m(z') = \frac{1}{M_m}\left[e^{ik_m(z_m - z')} + e^{ik_m d_m}\tilde{r}_{m-1,m}e^{-ik_m(z_{m-1}-z')}\right], \quad (21)$$

$$B_m(z') = \frac{1}{M_m}\tilde{r}_{m-1,m}\left[e^{-ik_m(z_{m-1}-z')} + e^{ik_m d_m}\tilde{r}_{m+1,m}e^{ik_m(z_m - z')}\right], \quad (22)$$

$$C_m(z') = \frac{1}{M_m}\tilde{r}_{m+1,m}\left[e^{ik_m(z_m - z')} + e^{ik_m d_m}\tilde{r}_{m-1,m}e^{-ik_m(z_{m-1}-z')}\right], \quad (23)$$

$$D_m(z') = \frac{1}{M_m}\left[e^{-ik_m(z_{m-1}-z')} + e^{ik_m d_m}\tilde{r}_{m+1,m}e^{ik_m(z_{m-1}-z')}\right], \quad (24)$$

where $\tilde{r}_{n\pm1,n}$ and $\tilde{t}_{n,m}$ are the generalized reflection and transmission coefficients, respectively [36]. The denominator is $M_m = 1 - \tilde{r}_{m+1,m}\tilde{r}_{m-1,m}e^{i2k_m d_m}$. The wave number in the perpendicular direction of layer n is $k_n = \sqrt{q_n^2 - k_\parallel^2}$.

For the electric field, we obtain

$$\nabla \times \nabla \times \mathbf{E} + \mu_0\varepsilon_0(1+\chi_E)\frac{\partial^2 \mathbf{E}}{\partial t^2} = -\mu_0\nabla\times\frac{\partial \mathbf{M}}{\partial t}. \quad (25)$$

For the TE mode, $\tilde{\mathbf{E}}^{(\mathrm{TE})} = (0, \tilde{E}_y, 0)^t$ is related to $\tilde{\mathbf{H}}^{(\mathrm{TE})}$ through Faraday's law. The $\nabla\nabla\cdot\mathbf{E}$ term on the left-hand side is incorporated with the boundary conditions. Thus, the solution of $\tilde{\mathbf{H}}^{(\mathrm{TE})} = (\tilde{H}_x, 0, \tilde{H}_z)^t$ is given by

$$\tilde{\mathbf{H}}^{(\mathrm{TE})}(\mathbf{k}_\parallel, z; \omega) = \tilde{\mathbf{H}}^{(\mathrm{TE})}_{\mathrm{inc}}(\mathbf{k}_\parallel, z; \omega) + \int dz' \bar{G}^{(\mathrm{TE})}(\mathbf{k}_\parallel, z, z'; \omega)\tilde{\mathbf{M}}(\mathbf{k}_\parallel, z'; \omega), \quad (26)$$

with

$$\bar{G}^{(\mathrm{TE})}(\mathbf{k}_\parallel, z, z'; \omega) = -\begin{pmatrix} \partial_z\partial_{z'} & 0 & ik_\parallel\partial_z \\ & & \\ -ik_\parallel\partial_{z'} & & k_\parallel^2 \end{pmatrix} \frac{ig(\mathbf{k}_\parallel, z, z'; \omega)}{2\sqrt{q(z')^2 - k_\parallel^2}} - \begin{pmatrix} 0 & & \\ & 0 & \\ & & 1 \end{pmatrix} \delta(z - z'), \tag{27}$$

where the scalar Green's function $g(\mathbf{k}_\parallel, z, z'; \omega)$ is the same as that for the TM mode in Eq. (20). The xx component of the second term is modified to eliminate singularity owing to the $\partial_z\partial_{z'}$ term.

The summation of Eqs. (19) and (27) gives the formal solution of the total field, Hence we obtain the total Green's function as the sum of Eqs. (19) and (27) as

$$\bar{G}(\mathbf{k}_\parallel, z, z'; \omega) = \bar{G}^{(\mathrm{TM})}(\mathbf{k}_\parallel, z, z'; \omega) + \bar{G}^{(\mathrm{TE})}(\mathbf{k}_\parallel, z, z'; \omega), \tag{28}$$

and the formal solution of the Maxwell's equations can be represented as

$$\tilde{\mathbf{H}}(\mathbf{k}_\parallel, z; \omega) = \tilde{\mathbf{H}}_{\mathrm{inc}}(\mathbf{k}_\parallel, z; \omega) + \int dz' \bar{G}(\mathbf{k}_\parallel, z, z'; \omega)\tilde{\mathbf{M}}(\mathbf{k}_\parallel, z'; \omega). \tag{29}$$

D. Self-consistent treatment

We formulate a general nonlocal response theory [37,38] for magnons. The electromagnetic fields $\tilde{\mathbf{H}}$ and $\tilde{\mathbf{E}}$, magnetization $\tilde{\mathbf{M}}$, and polarization $\tilde{\mathbf{P}}$ are determined self-consistently based on the constitutive equation (11) and the formal solution of the Maxwell's equations (29). For the Hamiltonian of Eqs. (6) and (7), the magnetic field described in the Maxwell's equations has to be expressed as $\tilde{\mathbf{h}} = \tilde{\mathbf{h}}_{\mathrm{inc}} + \tilde{\mathbf{h}}_{\mathrm{res}}$. The self-consistent relation is rewritten in matrix form: for the total and incident fields, the coefficients are introduced as

$$F_n = \int dz \frac{\tilde{\boldsymbol{\mu}}_n^\dagger(z)\tilde{\mathbf{h}}(z)}{E_{n,\mathbf{k}_\parallel} - \hbar\omega - i\gamma_m}, \tag{30}$$

$$f_n = \int dz \frac{\tilde{\boldsymbol{\mu}}_n^t(z)\tilde{\mathbf{h}}(z)}{E_{n,\mathbf{k}_\parallel} + \hbar\omega + i\gamma_m}, \tag{31}$$

$$X_n = \int dz \tilde{\boldsymbol{\mu}}_n^\dagger(z)\tilde{\mathbf{h}}_{\mathrm{inc}}(z), \tag{32}$$

$$x_n = \int dz \tilde{\boldsymbol{\mu}}_n^t(z)\tilde{\mathbf{h}}_{\mathrm{inc}}(z), \tag{33}$$

where the associated vectors $\mathbf{F} = (\{F_n\}, \{f_n\})^t$ and $\mathbf{X} = (\{X_n\}, \{x_n\})^t$. The dyadic Green's function yields the factors of the matrices as

$$A_{n,n'} = -\frac{\mu_0}{v}\int dz \int dz' \tilde{\boldsymbol{\mu}}_n^\dagger(z)\bar{G}(\mathbf{k}_\parallel, z, z'; \omega)\tilde{\boldsymbol{\mu}}_{n'}(z'), \tag{34}$$

$$a_{n,n'} = -\frac{\mu_0}{v}\int dz \int dz' \tilde{\boldsymbol{\mu}}_n^t(z)\bar{G}(\mathbf{k}_\parallel, z, z'; \omega)\tilde{\boldsymbol{\mu}}_{n'}^*(z'), \tag{35}$$

$$W_{n,n'} = -\frac{\mu_0}{v}\int dz \int dz' \tilde{\boldsymbol{\mu}}_n^\dagger(z)\bar{G}(\mathbf{k}_\parallel, z, z'; \omega)\tilde{\boldsymbol{\mu}}_{n'}^*(z'), \tag{36}$$

$$w_{n,n'} = -\frac{\mu_0}{v}\int dz \int dz' \tilde{\boldsymbol{\mu}}_n^t(z)\bar{G}(\mathbf{k}_\parallel, z, z'; \omega)\tilde{\boldsymbol{\mu}}_{n'}(z'). \tag{37}$$

Thus,

$$\bar{S}\mathbf{F} = \mathbf{X} \tag{38}$$

with

$$\bar{S} \equiv \begin{pmatrix} \bar{E} - (\hbar\omega + i\gamma_m)\bar{1} + \bar{A} & \bar{W}, \\ \bar{w} & \bar{E} + (\hbar\omega + i\gamma_m)\bar{1} + \bar{a} \end{pmatrix}. \tag{39}$$

Here $\bar{E}$ is a diagonal matrix based on eigenenergies. Notably, the interaction between magnons is described in the matrix through Green's function. The determinant of matrix $\bar{S}$ yields the dispersion relation of the MPs.

Even for magnetic materials with magnon excitation, the dielectric constant contributes to the microwave reflection and refraction. Although we focused on the linear response of magnons, the nonlocal self-consistent theory proposed herein for the magnons and radiative field played a significant role to enhance the magnonic antenna effect.

E. Model of the multilayer structure

For the proposed multilayered structure shown in Fig. 1(a), we assume two yttrium iron garnet (YIG) layers of 100 nm and 500 μm thickness. The two layers are separated by a 1-μm-thick gadolinium gallium garnet (GGG) layer, which is a paramagnetic insulator and standard material for heterostructures with YIG. A schematic of the structure is presented in Fig. 2(a). Thick YIG films are favorable for stronger MP coupling, which results in larger magnon currents. However, to ensure a suitable fabrication quality, it is important to verify that even a considerably thinner nanometer-order YIG film can function suitably under the magnonic antenna effect. Thus, we select a thickness of 100 nm, which can be processed using standard fabrication techniques. The thickness of the top

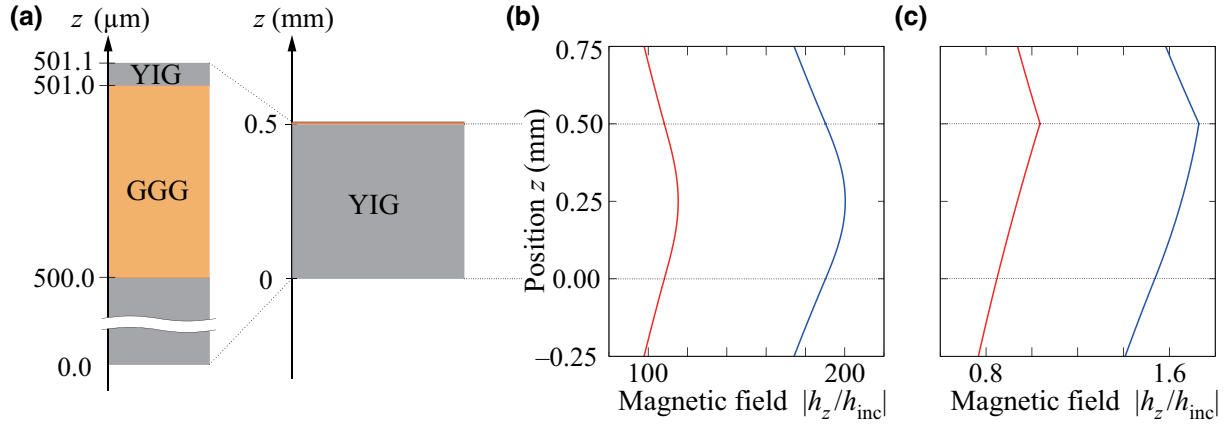

FIG. 2. (a) Schematic of the proposed multilayered structure cross section with a 100 nm YIG/1 μm GGG/500 μm YIG layered structure. (b),(c) Spatial profiles of the transverse (blue) and longitudinal magnetic fields (red lines) originating from the (b) thick- and (c) thin-layer magnons. The field amplitude is normalized by the incident field $h_{\rm inc}$. Other parameters are as follows: $\mu_0 M_s = 175$ mT, $\lambda_{\rm ex} = 1.76 \times 10^{-8}$ m, $\epsilon_M = 15$, $\epsilon_b = 12$, $H_0^{\rm (thin)} = 1.12 H_M$, and $H_0^{\rm (thick)} = 1.5 H_M$. The unit of the magnetic field is $H_M \equiv \hbar\omega_M/(g\mu_B\mu_0) = M_s$.

thin YIG layer is not essential for our claim in this study because thicknesses of 50 and 200 nm indicate the same results quantitatively. Although thicker YIG is better suited for a large magnon current, thinner is suitable for circuit fabrication.

The saturation magnetization is $\mu_0 M_s \simeq 175$ mT for YIG [39], where the frequency corresponding to magnetization is $\omega_M = g\mu_B\mu_0 M_s/\hbar \simeq 4.89 \times 2\pi$ GHz. Here, μ_B is the Bohr magneton, the g factor is $g = 2$, and the coherence length of the exchange interaction is $\lambda_{\rm ex} \simeq 1.76 \times 10^{-8}$ m. The dielectric constant is $\epsilon_M = 15$ for YIG [40] and $\epsilon_b = 12$ for GGG [41]. The nonradiative relaxation constant is set as $\gamma_m = 0.8$ MHz. The magnon is excited in each YIG layer, and the interlayer magnon-magnon interaction is attributed to the dipole-dipole interaction. An incident microwave $h_{\rm inc}$ is introduced onto the surface of the thick layer. The microwave is applied to the multilayered structure even for an in-plane wave number $k_\parallel$ larger than the wave number $q_0 = \omega/c$ in vacuum. This can be realized by utilizing an evanescent prism mode on the structure, or a fiber coupling at the edge surface. For the calculation of the fields inside and outside the sample, we place a field inside the thicker YIG layer and consider the boundary conditions of the microwave through Green's function to determine the self-consistent fields in other layers. We apply an in-plane gradient magnetic field with $H_0^{\rm (thin)} = 1.120 H_M$ and $H_0^{\rm (thick)} = 1.5 H_M$ to the thin and thick layers, respectively, to obtain level (anti)crossing of thin-layer magnons and thick-layer MPs. Here, we use $H_M \equiv \hbar\omega_M/(g\mu_B\mu_0)$ as a unit for the magnetic field. Such a spatial gradient of the magnetic field can be realized using micromagnets or current-induced fields. (The use of different magnetic materials for the two layers also offers similar level crossings.)

We emphasize on the role of the GGG layer. The GGG spacer layer enables the engineering of dispersion. Without the GGG layer, which means a single 500.1 μm YIG film, fabricated circuits of a (surface) 100-nm-thick layer cannot function because the magnon wave functions spread along the longitudinal direction and the spatial gradient of the applied magnetic field, which is indispensable for manipulating dispersion crossing, become ineffective. Moreover, the absence of a separation layer would leave a single YIG film, and the magnons become insensitive to the fabricated circuit because the hundred-nanometer-scale modulation of thickness is insignificant for the magnons in the millimeter-scale YIG film. Therefore, the GGG separation layer plays a critical role in the functioning of the proposed system. The thickness of the GGG layer should be greater than the penetration length of the magnons to disconnect the magnon wave functions in the two layers. A few nanometers on scale [42] of magnon decay length in NiO of YIG was reported, while a magnetic proximity effect was also reported between Co and YIG, with a few nm GGG layer [43]. During the spin information transport from YIG under a large magnetic field at low temperature, the spin diffusive length in GGG was approximately 2 μm [4]. Hence, we consider a 1-μm-thick GGG layer enough to separate the magnons in the two YIG layers at room temperature. On the other hand, the decay length of the spin dipole-dipole interaction for the magnon wave number under consideration is significantly greater than the aforementioned thickness. Hence, a micrometer-order modulation of the GGG layer thickness is insignificant for the magnonic antenna effect.

In the proposed structure, the waveguide modes and magnonic antenna effect impart the thin-layer MP transport with functionalities that are essential for practical

applications. In the following discussion we consider the waveguide mode in the structure with thickness d. In a case of a single thick film, the TE and TM waveguide modes are formed within $q < k_\parallel < q_0$, which decays exponentially in vacuum, where $q = q_0/\sqrt{\epsilon_M}$. The waveguide modes satisfy the condition $k_z d + \mathrm{Arg}(r_\xi) = n\pi$ for $\xi =$ TE, TM. Here, $k_z = \sqrt{q^2 - k_\parallel}$. The reflection coefficient r_ξ at the interfaces depends on the wave number $(k_\parallel, k_z)$. Here, n denotes the index of the waveguide mode, and the modes require millimeter-scale thickness, $d \simeq \pi/k_z \sim$ mm. Although this condition is slightly different for multilayer structures, the behavior of the mode remains qualitatively unaffected. When $k_\parallel > q_0$ (out of the light line), the incident light is an evanescent wave, hence, it is not effective for the MP application. While the thinner structure is better for a wide range $k_\parallel$ utilization, the thicker YIG is more desirable for the magnonic antenna effect to excite many magnons in the thick layer and transcribe the MP excitation to the thin layer. Then, we consider 500 μm for thick YIG layer to be safe for negative group velocity of propagating MPs and be enough strong MPs.

Note that we do not treat an optical antenna effect in our study. In our model, efficiency of light capturing of the thick layer is 100%, namely we do not explicitly consider the connection between the input light and waveguide modes and optical loss in the thick layer. The consideration of input light causes complicated elements that are not essential, and hence, we omit them in our model.

III. RESULTS AND DISCUSSION

In this section we discuss the dispersion relations of the MPs with a comparison between several multilayered structures. The forming of MPs enhances the group velocity. In the 100 nm YIG/1 μm GGG/500 μm YIG structure, the properties of the MPs in the thick layer are transcribed to those in the thin layers. Moreover, the density of the MPs in the thin layer is significantly enhanced by the magnonic antenna effect. The transcribed properties are tuned by applying external magnetic fields to the thin layer. Then, we obtain efficient and rich functionalized MPs even in the thin layer.

A. Induced fields by thick- and thin-layer magnons

In the proposed structure, the magnons in the thick and thin YIG layers induce both a longitudinal magnetic field and a transverse electromagnetic field. Figures 2(b) and 2(c) shows the amplitude of the transverse field. The longitudinal field results in an interlayer magnon-magnon interaction. The fields of the thick-layer magnons are almost symmetric in the z direction, whereas the transverse field of the thin-layer magnons exhibits a nonsymmetric behavior owing to the difference in dielectric constants. Hence, considering the nonlocal response of magnons is essential.

B. Dispersion relation of the magnon polaritos

Engineering the dispersion relation enables control over magnon propagation. To demonstrate this, we consider three types of layered systems with YIG: Structure I is a 500-μm-thick YIG film, Structure II is a 100 nm YIG/500 μm GGG, and Structure III is a 100 nm YIG/1 μm GGG/500 μm (proposed structure). The YIG layers exhibit in-plane magnetization. The magnonic antenna effect originates from the dispersion of the MPs in the thick YIG layer, and the waveguide modes require the system to possess a certain thickness.

Figures 3(a) and 3(b) present the dispersion relations $\omega^{(\alpha)}(k_\parallel)$ of the MPs in structures I and II, respectively, with α as an index of the MP branches. If a single 100 nm YIG film exists alone, the light-magnon coupling is negligible because the thickness of the layer is much thinner than the light wavelength and the light is hardly confined by the layer. Therefore, the dispersion is almost independent from the in-plane wave number $k_\parallel$ (not shown). In structure I, the bare magnon exhibits a negative slope [44]. The thick film spontaneously forms the TE and TM waveguide modes, which results in strong MPs and three dispersions in Fig. 3(a). We refer to these as the thick-layer upper, middle, and lower MPs [denoted as thick UMP, thick MMP, and thick LMP, respectively, in Fig. 3(a)]. At $0.06 < k_\parallel d < 0.20$, the group velocity $v_g^{(\alpha)} = \partial\omega^{(\alpha)}/\partial k_\parallel$ of the three MPs is significantly higher than that of the bare magnon. The in-plane wave number $k_\parallel$ can be tuned by adjusting the incident angle. With an increase in the incident angle, the propagation direction of the thick LMP changes around $k_\parallel d = 0.24$. This is an origin of rich functionalities of thin-layer MPs in the proposed structure (structure III). In structure II the dielectric layer sustains light (as an optical antenna effect), hence, the light-magnon coupling is enhanced. The dispersion exhibits direct coupling between the thin-layer magnons, which is almost flat at $\omega \approx 1.86\omega_M$, and the TE/TM modes. Their coupling strengths are evaluated as $\Delta_{\mathrm{TE}} \simeq 1.3 \times 10^{-3}\omega_M$ at $k_\parallel d \approx 0.096$ and $\Delta_{\mathrm{TM}} \simeq 3.0 \times 10^{-3}\omega_M$ at $k_\parallel d \approx 0.108$, respectively, from Fig. 3(b).

Structure III has two YIG layers and the MPs are formed in both layers separately. In the thick layer the MPs show qualitatively the same properties as those of the MPs in structure I. They are transcribed to the thin-layer MPs by the interlayer magnon-magnon interaction (longitudinal field) and a share of the waveguide modes (transverse field). Figure 3(c) shows the dispersions of the MPs in structure III. In the vicinity of dispersion crossing points, the thin-layer magnons couple strongly with the thick MMP at $k_\parallel d \approx 0.10$ and with the thick LMP at $k_\parallel d \approx$ 0.19 and 0.30. Then, the thick-layer MPs provide their functionality to the thin-layer magnons as the magnonic antenna effect. Even though the magnon-magnon coupling is present, the level splittings at the anti-crossings are almost the same as those in structure II. Thus, the

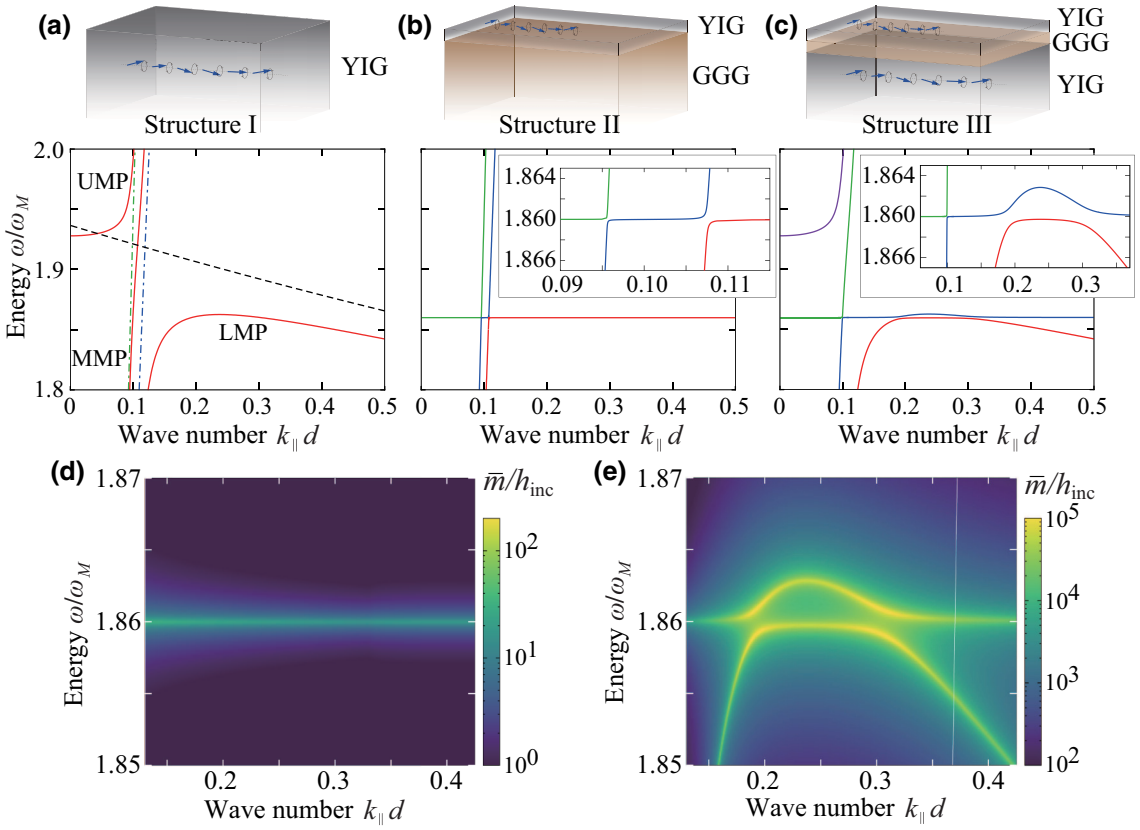

FIG. 3. (a),(b),(c) Dispersion relations $\omega^{(\alpha)}(k_\parallel)$ of the MPs in the single 500 μm YIG film (a, structure I); 100 nm YIG/500 μm GGG structure (b, structure II); and proposed structure, 100 nm YIG/1 μm GGG/500 μm YIG (c, structure III). Here α is an index of the MP branches. The corresponding structures are shown above the panels. The wave number is normalized by $d = 500$ μm. The YIG layers exhibit in-plane saturation magnetization. The other parameters are the same as those in Fig. 2. The external static magnetic fields are applied along the in-plane magnetization. The solid lines indicate the MPs in panels (a)–(c). In (a) the black dotted line indicates the bare magnon, and the blue and green dotted lines represent the TE and TM modes, respectively. In (b),(c) the colors of the solid lines are clearly distinguishable. The insets of (b),(c) present zoomed views. (d),(e) Magnetization amplitude $\bar{m}$ deviated from the saturation magnetization of the thin-layered YIG in structure II (d) and structure III (e), respectively. The amplitude is normalized by the incident magnetic field $h_{\rm inc}$. Along the dispersion of the MPs, the magnetization $\bar{m}$ is enlarged. A white line in (e) indicates the light line in the structure. In the right and left regions from the line, the waveguide modes are evanescent and propagating waves.

light-magnon coupling due to the waveguide modes is not enlarged by the magnonic antenna effect. Interestingly, at the latter two anticrossings, the MPs exhibit forward and backward propagation, respectively. The functionalities imparted to the thin-layer magnons can be tuned using the external magnetic fields.

To discuss the magnon current given by the group velocity and density, we consider the magnon density proportional to the magnetization amplitude of the deviation from the saturation magnetization, $\mathbf{m}(\mathbf{r}) = \mathbf{M}(\mathbf{r}) - \mathbf{M}_s$. Figures 3(d) and 3(e) present the spatial integral of the induced magnetization in the thin YIG layer, $\bar{m} = \sqrt{1/S_0 d_0 \int_{d_0} dz \int_{S_0} dxdy |\mathbf{m}(\mathbf{r})|^2}$, for structures II and III as functions of ω and $k_\parallel$, respectively. The enhancement in $\bar{m}$ means the generation of a large magnon density. Here, S_0 and d_0 denote the area of the YIG unit cell and the thickness of the thin layer, respectively. In structure II, although the induced magnetization $\bar{m}(k_\parallel, \omega)$ follows the dispersion of the bare magnon, the amplitude enhancement is up to $\bar{m}/h_{\rm inc} \sim 10^2$. In structure III, $\bar{m}$ is considerably increased up to $\bar{m}/h_{\rm inc} \sim 10^5$ owing to the interlayer magnon-magnon interaction appearing on the dispersions of the thin layer of the bare magnon and thick LMP. Hence, the magnonic antenna effect yields the enhancement of magnon density in the thin YIG and the transcription of rich functionalities of thick-layer MPs to thin-layer MPs, whereas the light-magnon coupling is almost irrelevant. This enhancement of $\bar{m}$ causes a large magnon current in the thin YIG. The enhancement should be discussed in a propagating region for the waveguide modes in the left of light line because a microwave incidence to the system by prism is ineffective in an evanescent region. Along the dispersion $\omega^{(\alpha)}(k_\parallel)$ in structure III, we plot the wave number dependence of the induced magnetization $\bar{m}^{(\alpha)}$ and the group velocity $v_g^{(\alpha)}$, as shown in Figs. 4(a) and 4(b),

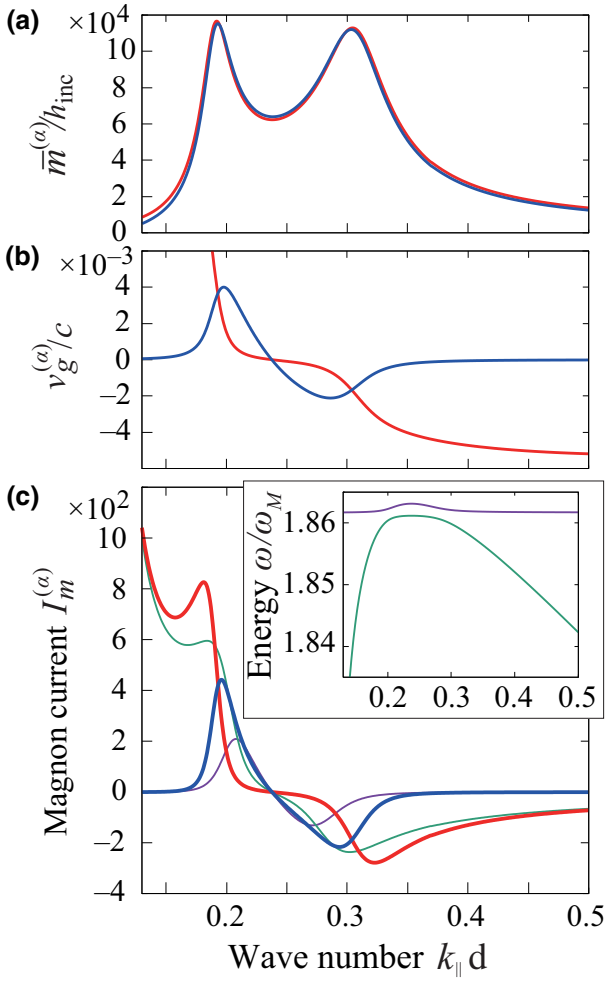

FIG. 4. Magnon current in the thin YIG layer of structure III. (a) Induced magnetization $\bar{m}^{(\alpha)}$ in Fig. 3(e) along with the dispersion of two MPs in Fig. 3(c). (b) Group velocity $v_g^{(\alpha)}$ of thin-layer MP dispersion, as shown in Fig. 3(c). The velocity is normalized by the velocity of light in vacuum, c. (c) The (normalized) magnon current $I_m^{(\alpha)}$ in the thin-layer MPs when external fields $H_0^{(\text{thin})} = 1.120H_M$ (thick lines) and $= 1.122H_M$ (thin lines) are applied. The red and blue lines in (a)–(c) denote the lowest and second MP branches in Fig. 3(c), respectively. The green and magenta lines and inset show $I_m^{(\alpha)}$ and the dispersion relation when $H_0^{(\text{thin})} = 1.122H_M$, respectively.

respectively. The magnon density in the thin YIG layer is enhanced owing to the strong coupling with the thick LMP. The MP velocity can be faster by more than 3×10^{-3} times the speed of light in vacuum, namely in the order of 10^6 m/s, which is 10^3 times the typical (exchange) magnon velocity [8,45–47]. Note that these enhancements of MPs are stronger when YIG layers are thicker. However, an increase of the system thickness shifts the light line [white line in Fig. 3(e)] to the left. Then, the strong MPs becomes in the evanescent region. Hence, 500 μm YIG is reasonable consideration.

C. Magnon current carried by the magnon polaritos

Figure 4(c) shows the magnon currents in the MPs, which are expressed as

$$I_m^{(\alpha)}(k_\parallel) = v_g^{(\alpha)}(k_\parallel) \times \bar{m}^{(\alpha)}(k_\parallel, \omega^{(\alpha)}(k_\parallel)). \tag{40}$$

Following the peaks of $\bar{m}^{(\alpha)}$ and the sign of $v_g^{(\alpha)}$, the magnon current in the thin YIG layer exhibits peak and dip behaviors at $k_\parallel d \approx 0.19$ and 0.30, respectively. Note that the large group velocity and the magnon current, far from the anticrossings, are attributed to the thick LMP. For the enlarged magnon current in the thin layer, we should focus on the vicinity of the anticrossings. Under applied static magnetic fields, $H_0^{(\text{thin})} = 1.120H_M$ and $H_0^{(\text{thick})} = 1.5H_M$, the incident angle of the microwave should be tuned from $k_\parallel d \approx 0.19$ to 0.30 to switch the magnon current direction. The distance between the peak and dip is rather large in this case. However, the distance can be reduced by controlling the shifts in the thin-layer magnon energy. Thus, two anticrossing points at the end can be modulated by tuning the applied field $H_0^{(\text{thin})}$ in the thin layer. We examine a sweep of the thin-layer magnon energy by $H_0^{(\text{thin})}$ up to the dispersion edge of the thick LMP.

Figures 5(a) and 5(b) demonstrate the magnon current $I_m^{(\alpha)}$ from the two MP branches, respectively. With a slight increase in $H_0^{(\text{thin})}$, the distance between the peaks and dips of $I_m^{(\alpha)}$ are reduced. At $H_0^{(\text{thin})} > 1.123H_M$, the peaks and dips are unified, and the magnon current is reduced significantly. The thin lines and the inset of Fig. 4(c) indicate the magnon current and dispersion, respectively, when $H_0^{(\text{thin})} \approx 1.122H_M$. The peak and dip are sufficiently detectable, and the sign can be altered by a slight shift in $k_\parallel$. This condition can be deemed appropriate for magnon current switching. When $H_0^{(\text{thin})}$ decreases, the distance between the peaks and dips increases. For a large $k_\parallel d$, the magnon-magnon interaction is suppressed owing to the exponential decay of the longitudinal field for short-wavelength microwaves. Then, the dip disappears when $H_0^{(\text{thin})}$ is reduced.

The dispersion exhibits anticrossing with the thick MMP at $k_\parallel d \approx 0.10$, shown in Fig. 3(c). The peak and dip of $I_m^{(\alpha)}$ for the thick LMP are broad, whereas the peak of the thick MMP is extremely sharp and isolated [outside the window in Fig. 4(c)]. This sharp peak is not considered here because the characteristics of such sharp peaks are not useful for practical applications. If the magnon circuit is fabricated in the thin layer, as shown in Fig. 1(b), the internal magnetic field and magnetization would be slightly varied. The sharp peak is highly sensitive to such changes, hence, it is difficult to utilize.

For the proposed structure illustrated in Fig. 1(b), some parts of the YIG are removed. In those areas, the dispersion of MPs is almost equivalent to that shown in Fig. 3(a).

The thick LMP may induce a large magnon current. However, at the dispersion edge ($k_\parallel d \simeq 0.24, \omega/\omega_M \simeq 1.863$), the magnon current is suppressed due to low velocity of the magnons. Thus, the leakage magnon current is expected to reduce. This is also an important advantage of the proposed structure. Details regarding the behaviors of magnons in the processed thin layer cannot be obtained by referring only to the present study; these behaviors should be elucidated based on corresponding models. Thus, we are currently investigating the issue using numerical techniques based on nonlocal response theory.

D. Coherence length and figure of merit

The coherence length $\lambda_m^{(\alpha)}$ of the MPs provides a typical length scale for an information transport by magnons and a limitation of device application because the proposed system does not work well when the coherent length of the MPs is much shorter than the device. Here $\lambda_m^{(\alpha)}$ can be estimated from the group velocity $v_g^{(\alpha)}$ of MPs and their radiative damping $\Gamma_m^{(\alpha)}$ deduced from the imaginary component of radiative energy of the MPs, $\Gamma_m^{(\alpha)} = -\mathrm{Im}(\hbar\omega^{(\alpha)})$.

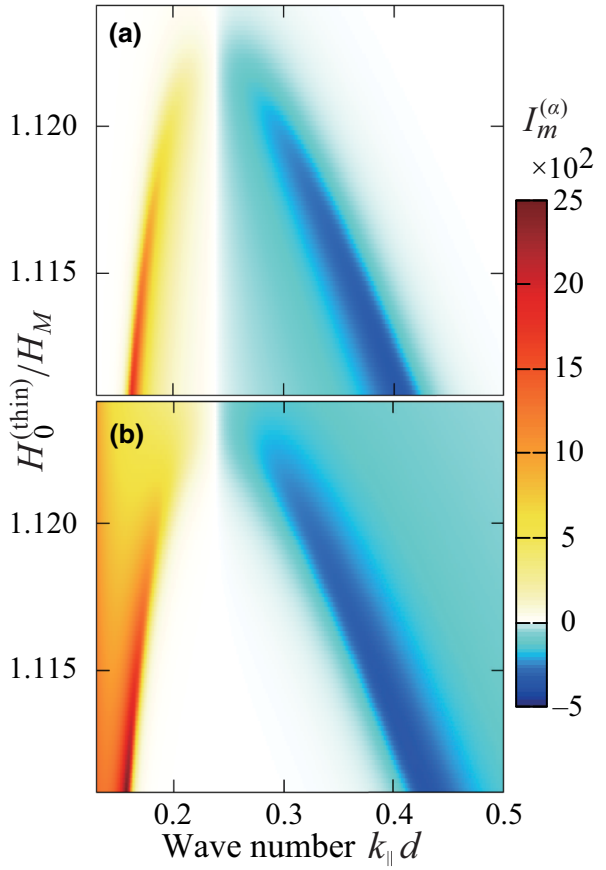

FIG. 5. Colored plot of magnon current I_m in the thin YIG layer of structure III, from the second (a) and lowest (b) branches of the thin-layer MPs in a plane of the external magnetic field represented as $H_0^{(\mathrm{thin})}$ and the in-plane wave number $k_\parallel d$.

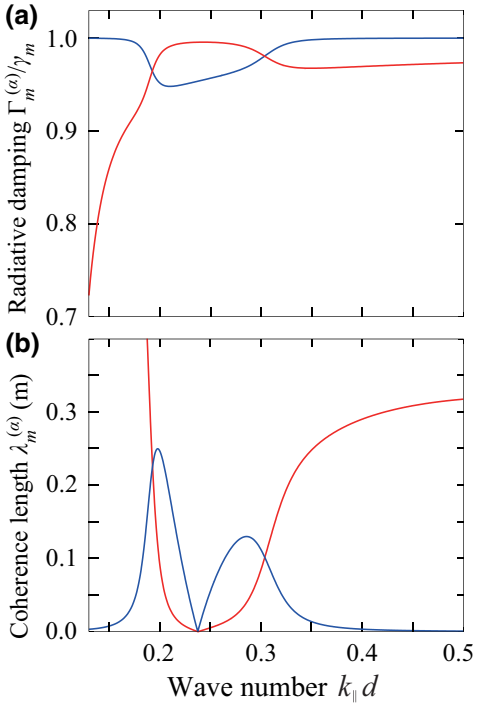

FIG. 6. (a) Radiative damping $\Gamma_m^{(\alpha)}(k_\parallel)$ and (b) coherence length $\lambda_m^{(\alpha)}$ of the MPs in structure III. The wave number is normalized by $d = 500$ μm. The colors of the solid lines correspond to those of Fig. 3(c).

Figure 6(a) exhibits the radiative damping $\Gamma_m^{(\alpha)}$ of the MPs in structure III. The damping of bare magnons is given by the nonradiative relaxation constant γ_m in Eq. (10). When the light-magnon coupling is enhanced and the MPs are formed, the coherence time $\tau_m^{(\alpha)} = \hbar/\Gamma_m^{(\alpha)}$ is enlarged. In Fig. 6(a) the lines roughly follow a constant value at $\Gamma_m^{(\alpha)} = \gamma_m$ attributing to the bare magnon and an exponential increase due to the thick LMP except at the vicinity of two anticrossing points $k_\parallel d \approx 0.19$ and ≈ 0.30. For the thin-layer MPs, the coherence time is enlarged around the anticrossings. Figure 6(b) shows $\lambda_m^{(\alpha)} = v_g^{(\alpha)}\tau_m^{(\alpha)}$ for structure III. Around the anticrossing points ($k_\parallel d = 0.19$ and 0.30), the coherence length is increased up to 200 mm, which is much longer than a typical coherence length of magnons. For example, the coherence length is 1.2 mm in Ref. [48], and summarized in a recent review [49]. Such a long coherence length is crucially useful for device applications. Note that in our model, the microwave is maintained in the structure, hence, the coherence length is overestimated. However, the waveguide modes give a long relaxation time and a 100 times enhancement of the coherence length by forming the MPs provides an essential idea.

From the radiative damping for the MPs, we estimate the figure of merit for the magnonic antenna effect. The magnonic antenna effect serves the rich functionalities and

large density of the MPs in the thin YIG layer. Hence, the figure of merit should be measured by the ratio between the damping of thick-layer MPs and the coupling strength of the MPs, namely the level spacing between the dispersions of the thick and thin MPs. Then, we roughly estimate the figure of merit from Figs. 3(c) and 6(a). The strength of the MPs is $\Delta \simeq 1.76\omega_M \simeq 54.0$ MHz at $k_\parallel d = 0.19$ and $\Delta \simeq 1.78\omega_M \simeq 54.5$ MHz at $k_\parallel d = 0.30$. The radiative damping is roughly $\Gamma_m^{(\alpha)} \sim \gamma_m = 0.8$ MHz. Therefore, the figure of merit is estimated as $\Delta/\Gamma_m \sim 65$, which suggests a high efficiency of the magnonic antenna effect.

IV. CONCLUSIONS

The magnon is a promising candidate for low-energy-consumption devices. To ensure effective device operation, the magnon current should be increased by increasing the density and velocity and acquiring switchable control over the direction of the current. One method to increase the velocity of the magnon is the formation of MPs. However, the light-magnon coupling is inherently weak.

To address this bottleneck, we propose a multilayered magnetic structure to demonstrate a large and switchable magnon current in the integrable thin magnetic layer. We consider two crucial mechanisms: waveguide modes and a magnonic antenna effect. The large magnon current and its switchable functionality are supported by these two phenomena. The formation of the waveguide mode is attributed to the spatial structure of the dielectric constant, which considerably enhances the light-magnon coupling caused by the spatial interplay between the magnons and microwaves. The magnonic antenna effect, originating from the thickness of YIG and the magnon-magnon interaction (longitudinal field), increases the excited magnon densities in the thin layer and transcribes the functionality of the thick-layer MPs to the nanoscale thin-layer MPs. By analyzing the dispersion relations of the MPs in this system based on nonlocal response theory, we exhibited an enlarged and switchable magnon current in the nanometer-scale thin film. Then, we demonstrate that the proposed multilayered structure can successfully exhibit the desired features mentioned above. The magnonic antenna effect arising from the thick LMP produces a broad peak and dip in the magnon current as a function of the incident angle. This is desirable for circuit fabrication in the thin layer. Moreover, from the radiative damping of MPs, we evaluate the coherence length for the MP transport and the figure of merit for the magnonic antenna effect. The evaluations indicate high efficiency of our proposed structure as magnonic devices. Our proposed approach thus presents the intriguing possibility of developing advanced magnonic technologies.

ACKNOWLEDGMENTS

This work is supported in part by JSPS KAKENHI 16H06504 in Scientific Research on Innovative Areas Nano-Material Optical-Manipulation," JSPS KAKENHI 18K13484 and 18H01151. T.Y. is supported by the Toyota Riken Scholar from the Toyota Physical and Chemical Research Institute.

[1] Y. Kajiwara, K. Harii, S. Takahashi, J. Ohe, K. Uchida, M. Mizuguchi, H. Umezawa, H. Kawai, K. Ando, K. Takanashi, S. Maekawa, and E. Saitoh, Transmission of electrical signals by spin-wave interconversion in a magnetic insulator, Nature **464**, 262 (2010).

[2] A. V. Chumak, A. A. Serga, and B. Hillebrands, Magnon transistor for all-magnon data processing, Nat. Commun. **5**, 4700 (2014).

[3] A. V. Chumak, V. I. Vasyuchka, A. A. Serga, and B. Hillebrands, Magnon spintronics, Nat. Phys. **11**, 453 (2015).

[4] K. Oyanagi, S. Takahashi, L. J. Cornelissen, J. Shan, S. Daimon, T. Kikkawa, G. E. W. Bauer, B. J. van Wees, and E. Saitoh, Spin transport in insulators without exchange stiffness, Nat. Commun. **10**, 4740 (2019).

[5] Y. Tabuchi, S. Ishino, A. Noguchi, T. Ishikawa, R. Yamazaki, K. Usami, and Y. Nakamura, Coherent coupling between a ferromagnetic magnon and a superconducting qubit, Science **349**, 405 (2015).

[6] D. Lachance-Quirion, S. P. Wolski, Y. Tabuchi, S. Kono, K. Usami, and Y. Nakamura, Entanglement-based single-shot detection of a single magnon with a superconducting qubit, Science **367**, 425 (2020).

[7] X. Zhang, C.-L. Zou, N. Zhu, F. Marquardt, L. Jiang, and H. X. Tang, Magnon dark modes and gradient memory, Nat. Commun. **6**, 8914 (2015).

[8] C. Liu, J. Chen, T. Liu, F. Heimbach, H. Yu, Y. Xiao, J. Hu, M. Liu, H. Chang, T. Stueckler, S. Tu, Y. Zhang, Y. Zhang, P. Gao, Z. Liao, D. Yu, K. Xia, N. Lei, W. Zhao, and M. Wu, Long-distance propagation of short-wavelength spin waves, Nat. Commun. **9**, 738 (2018).

[9] C. Liu, S. Wu, J. Zhang, J. Chen, J. Ding, J. Ma, Y. Zhang, Y. Sun, S. Tu, H. Wang, P. Liu, Ch. Li, Y. Jiang, P. Gao, D. Yu, J. Xiao, R. Duine, M. Wu, C.-W. Nan, J. Zhang, and H. Yu, Current-controlled propagation of spin waves in antiparallel, coupled domains, Nat. Nanotech. **14**, 691 (2019).

[10] Y. Onose, T. Ideue, H. Katsura, Y. Shiomi, N. Nagaosa, and Y. Tokura, Observation of the magnon Hall effect, Science **329**, 297 (2010).

[11] R. Matsumoto, R. Shindou, and S. Murakami, Thermal Hall effect of magnons in magnets with dipolar interaction, Phys. Rev. B **89**, 054420 (2014).

[12] S. Murakami and A. Okamoto, Thermal Hall effect of magnons, J. Phys. Soc. Jpn. **86**, 011010 (2017).

[13] Y. Cao, P. Yan, H. Huebl, S. T. B. Goennenwein, and G. E. W. Bauer, Exchange magnon-polaritons in microwave cavities, Phys. Rev. B **91**, 094423 (2015).

[14] Y. Tabuchi, S. Ishino, T. Ishikawa, R. Yamazaki, K. Usami, and Y. Nakamura, Hybridizing Ferromagnetic Magnons and Microwave Photons in the Quantum Limit, Phys. Rev. Lett. **113**, 083603 (2014).

[15] X. Zhang, C.-L. Zou, L. Jiang, and H. X. Tang, Strongly Coupled Magnons and Cavity Microwave Photons, Phys. Rev. Lett. **113**, 156401 (2014).

[16] Y.-P. Wang, G.-Q. Zhang, D. Zhang, T.-F. Li, C.-M. Hu, and J. Q. You, Bistability of Cavity Magnon Polaritons, Phys. Rev. Lett. **120**, 057202 (2018).

[17] P. Hyde, B. M. Yao, Y. S. Gui, G.-Q. Zhang, J. Q. You, and C.-M. Hu, Direct measurement of foldover in cavity magnon-polariton systems, Phys. Rev. B **98**, 174423 (2018).

[18] D. Zhang, X.-Q. Luo, Y.-P. Wang, T.-F. Li, and J. Q. You, Observation of the exceptional point in cavity magnon-polaritons, Nat. Commun. **8**, 1368 (2017).

[19] X. Zhang, K. Ding, X. Zhou, J. Xu, and D. Jin, Experimental Observation of an Exceptional Surface in Synthetic Dimensions with Magnon Polaritons, Phys. Rev. Lett. **123**, 237202 (2019).

[20] M. Harder, Y. Yang, B. M. Yao, C. H. Yu, J. W. Rao, Y. S. Gui, R. L. Stamps, and C.-M. Hu, Level Attraction Due to Dissipative Magnon-Photon Coupling, Phys. Rev. Lett. **121**, 137203 (2018).

[21] P.-C. Xu, J. W. Rao, Y. S. Gui, X. Jin, and C.-M. Hu, Cavity-mediated dissipative coupling of distant magnetic moments: Theory and experiment, Phys. Rev. B **100**, 094415 (2019).

[22] W. Yu, J. Wang, H. Y. Yuan, and J. Xiao, Prediction of Attractive Level Crossing via a Dissipative Mode, Phys. Rev. Lett. **123**, 227201 (2019).

[23] J. W. Rao, C. H. Yu, Y. T. Zhao, Y. S. Gui, X. L. Fan, D. S. Xue, and C.-M. Hu, Level attraction and level repulsion of magnon coupled with a cavity anti-resonance, New J. Phys. **21**, 065001 (2019).

[24] J. W. Rao, S. Kaur, B. M. Yao, E. R. J. Edwards, Y. T. Zhao, X. Fan, D. Xue, T. J. Silva, Y. S. Gui, and C.-M. Hu, Analogue of dynamic Hall effect in cavity magnon polariton system and coherently controlled logic device, Nat. Commun. **10**, 2934 (2019).

[25] N. J. Lambert, J. A. Haigh, S. Langenfeld, A. C. Doherty, and A. J. Ferguson, Cavity-mediated coherent coupling of magnetic moments, Phys. Rev. A **93**, 021803(R) (2016).

[26] L. Bai, M. Harder, P. Hyde, Z. Zhang, C.-M. Hu, Y. P. Chen, and J. Q. Xiao, Cavity Mediated Manipulation of Distant Spin Currents Using a Cavity-Magnon-Polariton, Phys. Rev. Lett. **118**, 217201 (2017).

[27] B. Zare Rameshti and G. E. W. Bauer, Indirect coupling of magnons by cavity photons, Phys. Rev. B **97**, 014419 (2018).

[28] Z. Zhang, M. O. Scully, and G. S. Agarwal, Quantum entanglement between two magnon modes via Kerr nonlinearity driven far from equilibrium, Phys. Rev. Res. **1**, 023021 (2019).

[29] J. Li and S.-Y. Zhu, Entangling two magnon modes via magnetostrictive interaction, New J. Phys. **21**, 085001 (2019).

[30] M. Kostyleva and A. A. Stashkevich, Proposal for a microwave photon to optical photon converter based on traveling magnons in thin magnetic films, J. Magn. Magn. Mater. **484**, 329 (2019).

[31] N. Zhu, X. Zhang, X. Han, C.-L. Zou, C. Zhong, C.-H. Wang, L. Jiang, and H. X. Tang, Waveguide cavity optomagnonics for microwave-to-optics conversion, Optica **7**, 1291 (2020).

[32] T. Yu, X. Zhang, S. Sharma, Y. M. Blanter, and G. E. W. Bauer, Chiral coupling of magnons in waveguides, Phys. Rev. B **101**, 094414 (2020).

[33] T. Holstein and H. Primakoff, Field dependence of the intrinsic domain magnetization of a ferromagnet, Phys. Rev. **58**, 1098 (1940).

[34] R. Kubo, Statistical-mechanical theory of irreversible processes. I. General theory and simple applications to magnetic and conduction problems, J. Phys. Soc. Jpn. **12**, 570 (1957).

[35] K. Cho, *Optical Response of Nanostructures: Microscopic Nonlocal Theory Springer Series in Solid-State Sciences* (Springer-Verlag, Tokyo, 2003).

[36] W. C. Chew, *Waves and Fields in Inhomogeneous Media IEEE PRESS Series on Electromagnetic Waves* (IEEE Press, New York, 1995).

[37] T. Kinoshita, T. Matsuda, T. Takahashi, M. Ichimiya, M. Ashida, Y. Furukawa, M. Nakayama, and H. Ishihara, Synergetic Enhancement of Light-Matter Interaction by Nonlocality and Band Degeneracy in ZnO Thin Films, Phys. Rev. Lett. **122**, 157401 (2019).

[38] H. Ishihara, *Comprehensive Nanoscience and Nanotechnology 2nd Edition* Vol. **4**, p. 323, Nanoscale Optical Response (Academic Press) 2019.

[39] A. Prabhakar and D. D. Stancil, *Spin Waves: Theory and Application* (Springer, 2009).

[40] K. Sadhana, R. S. Shinde, and S. R. Murthy, Synthesis of nonocrystaline YIG using microwave-hydrothermal method, Int. J. Mod. Phys. B **23**, 3637 (2009).

[41] K. Lal and H. K. Jhans, The dielectric constant of gadolinium gallium garnet and α-Al_2O_3 single crystals, J. Phys. C: Solid State Phys. **10**, 1315 (1977).

[42] C. Y. Guo, C. H. Wan, X. Wang, C. Fang, P. Tang, W. J. Kong, M. K. Zhao, L. N. Jiang, B. S. Tao, G. Q. Yu, and X. F. Han, Magnon valves based on YIG/NiO/YIG all-insulating magnon junctions, Phys. Rev. B **98**, 134426 (2018).

[43] B. B. Krichevtsov, A. M. Korovin, S. V. Gastev, S. M. Suturin, K. V. Mashkov, M. Sawada, and N. S. Sokolov, Magnetization reversal in Co/GGG/YIG/GGG (111) nanoheterostructures: Interlayer magnetic coupling and orange peel effect, J. Magn. Magn. Mater. **502**, 166542 (2020).

[44] B. A. Kalinikos and A. N. Slavin, Theory of dipole-exchange spin wave spectrum for ferromagnetic films with mixed exchange boundary conditions, J. Phys. C: Solid State Phys. **19**, 7013 (1986).

[45] H. Xia, P. Kabos, R. A. Staudinger, C. E. Patton, and A. N. Slavin, Velocity characteristics of microwave-magnetic-envelope solitons, Phys. Rev. B **58**, 2708 (1998).

[46] H. Yu, R. Huber, T. Schwarze, F. Brandl, T. Rapp, P. Berberich, G. Duerr, and D. Grundler, High propagating velocity of spin waves and temperature dependent damping in a CoFeB thin film, Appl. Phys. Lett. **100**, 262412 (2012).

[47] K. Yamanoi, S. Yakata, T. Kimura, and T. Manago, Spin wave excitation and propagation properties in a permalloy film, Jpn. J. Appl. Phys. **52**, 083001 (2013).

[48] H. Qin, Sampo J. Hämäläinen, K. Arjas, J. Witteveen, and S. van Dijken, Propagating spin waves in nanometer-thick yttrium iron garnet films: Dependence on wave vector, magnetic field strength, and angle, Phys. Rev. B **98**, 224422 (2018).

[49] G. Schmidt, C. Hauser, P. Trempler, M. Paleschke, and E. Th. Papaioannou, Ultra thin films of yttrium iron garnet with very low damping: A review, Phys. Status Solidi B **257**, 1900644 (2020).